Model validation for heavily damped structures. Application to a windshield joint.

Etienne Balmes[1,2]**, Mathieu Corus**[2]**, Sylvain Germès**[3]
[1]SDTools, 44 Rue Vergniaud, 75013 Paris, France
[2]Ecole Centrale Paris, MSSMat, 92295 Chatenay Malabry, France
[3]PSA Peugeot Citroen, 78943 Velizy, France
balmes@sdtools.com

Abstract

The use of damping augmentation concepts is spreading, thus motivating the need for design and validation methodologies. The frequency and temperature dependence of viscoelastic materials pose the challenge of correlating the response at multiple operating conditions. The fact that each mode is affected differently by the viscoelastic treatments is another difficulty. The paper first presents test results, at multiple temperatures, on a structure representative of a windshield with a damped joint. Then after a short reminder of numerical methodologies used to obtain response predictions, issues with the use of pole frequency and damping ratio for model correlation are illustrated.

1 Introduction

Devices using viscoelastic materials are often considered to enhance damping levels in vibrating structures in automotive, aerospace and energy applications. These designs often include parameters such as viscoelastic material thickness, position or properties that can vary over wide parametric ranges and only lead to good performance in relatively narrow operating ranges. Finding an efficient operating point thus requires parametric models where the treatment properties can easily be varied. Model validation is particularly important and yet challenging since temperature and frequency dependence need to be taken into account and each mode is affected differently by the treatment.

PSA Peugeot-Citroen has developed new concepts for windshield vibration damping trough the joints rather than using the traditional approach of damping material selection for the laminated glass. The experiment described in section 2 and used to illustrate this paper was motivated by the need to validate the joint models in such concepts. The test analysis correlation presented in the section is relatively good but poses many questions which the rest of the study addresses.

Section 3 summarizes procedures used to model the frequency and temperature dependence of viscoelastic materials and choices typically made to mesh viscoelastic treatments. Model reduction techniques, which are necessary to deal with the computational challenge posed by the proper representation of viscoelastic behavior, are then addressed.

Section 4 first recalls the equations associated with spectral decompositions. It is then shown that poles and modulus cannot be directly related in the considered applications. Since pole damping and frequencies remains the easiest correlation objective for damping validation, one proposes to use modal filters to extract modes. This works reasonably well for separated modes in both test and analysis but fails in tests when the modal density increases. Attempts to use output error identification techniques were found to give unreliable results in the same frequency range. The study then concludes by showing, using simple numerical illustration, that indeed there are unicity and bias problems with identification procedures.

2 Experiment representative of windshield joints

2.1 Test configuration

Two test cases are considered in this study. A structure dynamically representative of a windshield with a $500 \times 400 \times 0.5$ mm panel glued onto a aluminum frame shown in figure 2. The glue is a SMACTANE 50 band of section 10×4 mm (see figure 5 for properties). A "simplified" test corresponding to a cut of the full model is shown in figure 2. The joint is placed on a 2 mm plate that is representative of panel thicknesses found for windshield connection surfaces.

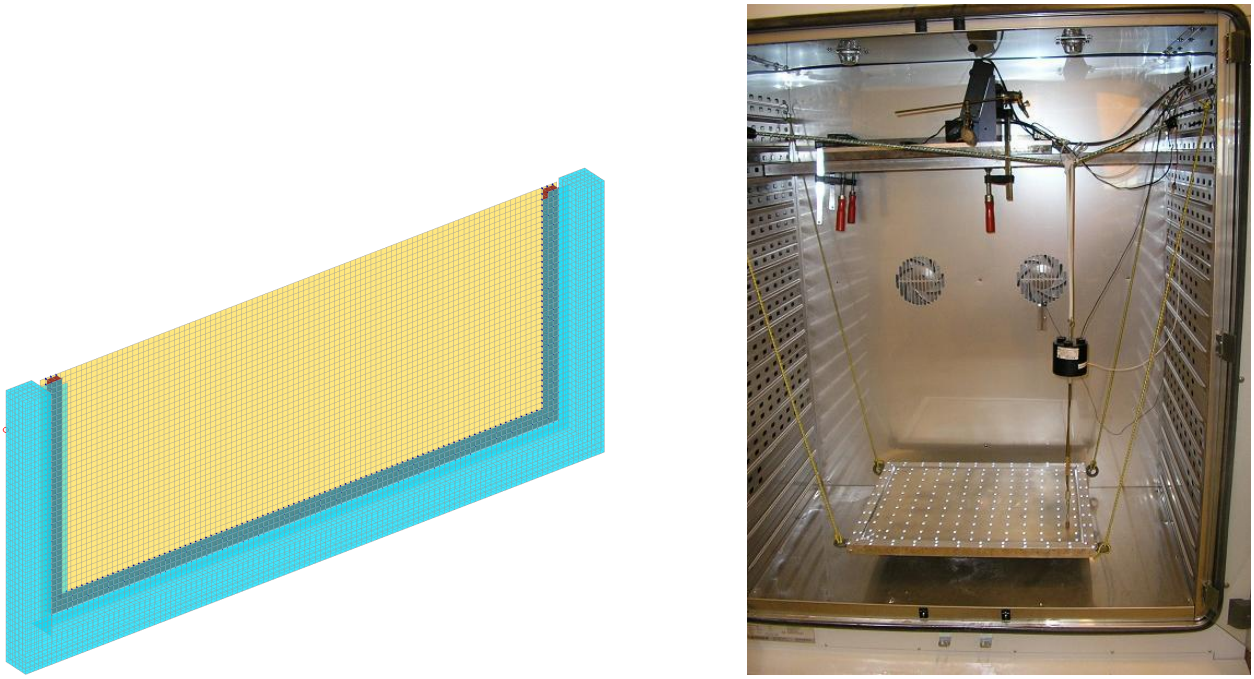

Figure 1: Test representative of a windshield glued onto its frame. Half model and photo of the test setup.

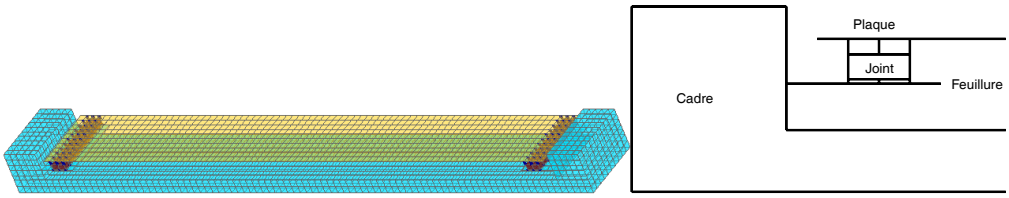

Figure 2: Simplified *slice* test.

The aluminum frames and plate were carefully manufactured to limit initial correlation errors to the effects in the joint model. The components where tested before being connected by the joint and initial correlation gave good results with less than 2 % error on predicted modal frequencies.

The tests where performed in an environmental chamber allowing a precise temperature control. 49 point where used for the slice and 223 for the frame. The optical scanner was placed in the chamber while the single point Polytech vibrometer was kept outside. Free-free conditions where approximated using bungee cords, which added some damping but also gave a temperature dependent static position which implied optical realignment. The slice was tested at 15, 25 and 35 C, the frame was also tested at 5 C. Data acquisition with a Photon system and scanner alignment where automatically controlled using a custom MATLAB application.

2.2 Test/analysis correlation

Figure 3 illustrates the good level of correlation found. Overall levels are well matched over the whole frequency band. The blue and green curves in the computed transfer are obtained with 2% and 0.2% loss factors in the frame respectively. The spread gives an idea of the how much of the difference in correlation could be due to external effects. In reality the bungee cords probably contribute most of the damping not due to the joint, but this contribution was not properly characterized.

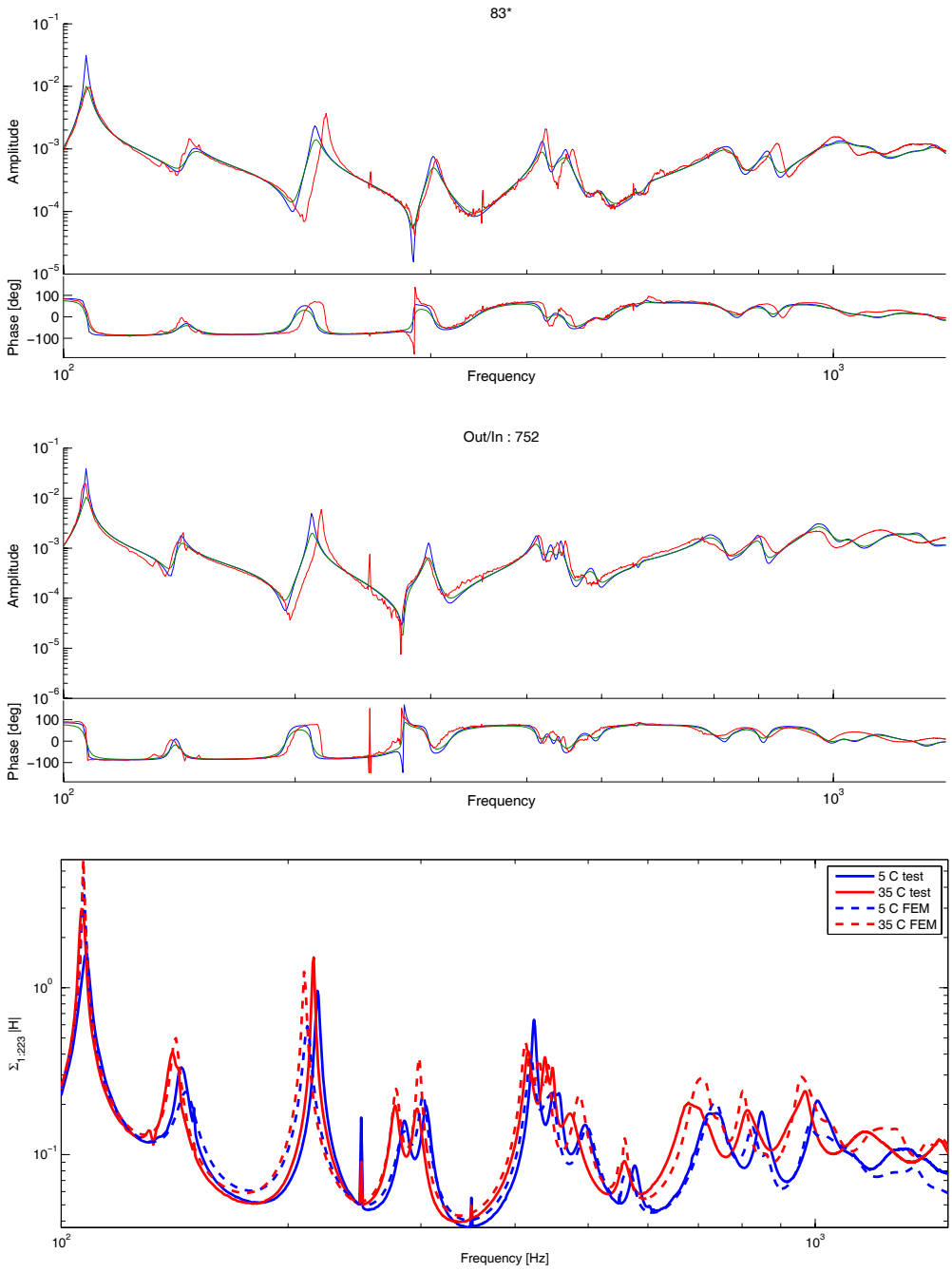

Figure 3: Test and analysis sample transfers and sum of transfers at 5 and 35 C (frame test)

Figure 4 gives a correlation for the first eight modes. These modes are not in the range where the treatment becomes really efficient but pole identification in that range was not possible for reasons that will be discussed

in later sections.

The general correlation is deemed to be quite good although the temperature trends are never reproduced exactly. Two FEM predictions are obtained using two separate material characterizations. This gives an idea of the difficulty of ensuring that the simulation is performed using characteristics that are close to those of the actual material. The significantly higher test damping on the first mode is attributed to dissipation in the bungee cords.

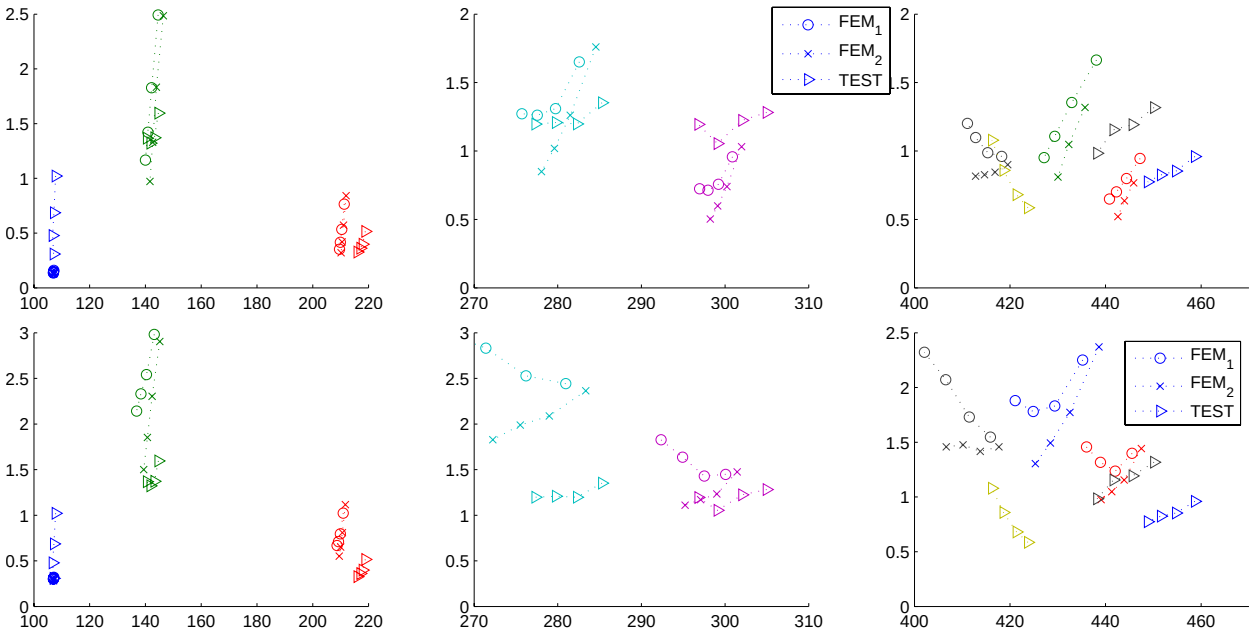

Figure 4: Pole correlation at 5, 15, 25, 35 C for the frame model and test.

3 Representing viscoelastic materials in dynamic models

3.1 Modeling issues

This section summarizes the main modeling issues pertinent in this study. More details can be found in Ref.[1]. For a selection of materials, indexed m, and using the fact that element stiffness depend linearly on the considered moduli, one can represent the dynamic stiffness matrix of a viscoelastic structure as a linear combination of constant matrices

$$[Z(E_m, s)] = Ms^2 + K_e + \sum_m \frac{\Lambda_m(s, T, \sigma_0)}{\Lambda_{m0}} K_{vm}(\Lambda_{m0}) \tag{1}$$

Possibly all moduli could be independent. In most applications, the stiffness is however dominated by either shear or compression. In free layers or support blocks, compression is dominant and the behavior of the damping device is dictated by the equivalent stiffness $k_v = Eh$ (compression modulus times height for free layer treatments). In constrained layer damping or shear struts, the viscoelastic stiffness is given by $k_v = GS/h$ with G the shear modulus, S the viscoelastic surface and h its thickness. In design phases a nominal value of G is used with a constant loss factor (typically 1) [2]. One then assembles the matrices for the elastic K_e and viscoelastic K_v parts and considers the parameterized dynamics stiffness given by

$$[Z(k_v, s)] = \left[Ms^2 + K_e + \tfrac{k_v}{k_{v0}}[K_v]\right] \tag{2}$$

In validation phases, one assumes that either shear of compression dominates and considers the frequency dependence of either the shear or Young's modulus and generally approximates the true variation of the other components using a constant real Poisson's ratio. Note that effects linked to the near incompressibility of some viscoelastic materials are known to have strong influence, but proper material characterization is then also very difficult.

Figure 5 for example shows the nomogram of the material used in the experiments. This figure assumes the validity of the frequency temperature superposition principle where the modulus is assumed to be a function of the reduced frequency $\omega\alpha(T)$ rather than a function of two independent variables ω and T. This principle is reasonably verified in many material tests and thus commonly used. It is also the only acceptable approach to extrapolate material properties in frequency ranges above 1 kHz where no dynamic material analyzer exists.

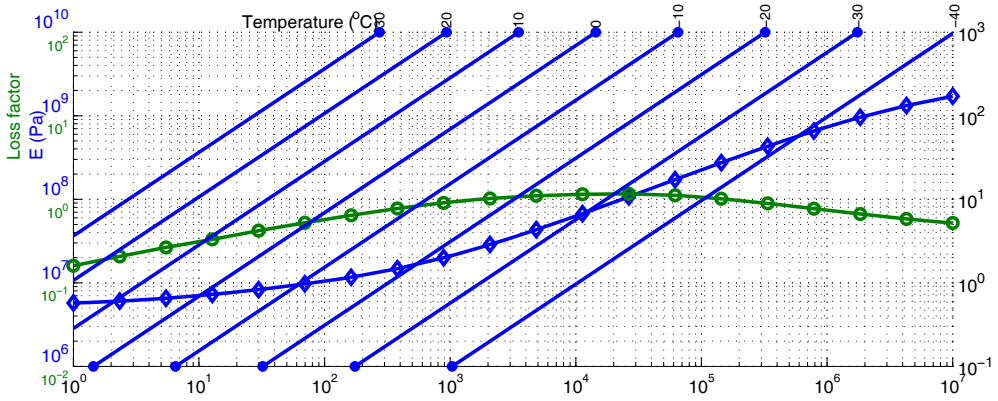

Figure 5: Nomogram for Smactane 50 material (www.smac.fr).

In most damping enhancement applications, viscoelastic materials are used in conjunctions with metals. Bending of the viscolastic layers is thus rarely dominant so that volume elements can be used appropriately to represent the strain energy. For classical free layer configurations, one can show that the composite model and a shell/volume model give nearly identical predictions. For constrained layer damping, shell/volume/shell models are appropriate even though the aspect ratio of the volumes elements used for the intermediate viscoelastic layer is out of normally accepted ranges [3, 1].

3.2 Solving for responses : reduction and parametric studies

To simulate the dynamic response it is not useful and rarely possible from a numerical cost standpoint to use direct frequency response computations by factoring (1). Model reduction methods (modal analysis, substructuring, component mode synthesis, ...) seek an approximate solution within a restricted subspace. One thus assumes

$$\{q\}_{N\times 1} = [T]_{N\times NR}\{q_R\}_{NR\times 1} \tag{3}$$

and seek solution of the full model forced response equation whose projection on the dual subspace T^T is zero (this congruent transformation corresponds to a Ritz-Galerkin analysis). Transfer functions are thus approximated by

$$[H(s)] = [c]\left(Z(s)\right)^{-1}[b] \approx [cT]\Big[T^T Z(s) T\Big]^{-1}\Big[T^T b\Big] \tag{4}$$

One can note that for a non-singular transformation T (when $\{q\} = [T]\{q_R\}$ is bijective) the input u / output y relation is preserved. One says that the transfer functions are objective quantities (they are physical quantities that are uniquely defined) while DOFs q are generally not objective.

Classical bases used for model reduction combine modes and static responses to characteristic loads [4]. Bases containing free modes and static responses to applied loads $\{b\}$

$$[T] = \left[[\phi_1 \dots \phi_{NM}] \quad \left[[K]^{-1}[b] - \sum_{j=1}^{NR} \frac{[c]\{\phi_j\}\{\phi_j\}^T[b]}{\omega_j^2} \right] \right] \tag{5}$$

have been used component mode synthesis (component model reduction to prior to a coupled system prediction) by Rubin [5], MacNeal [6], and many others. In the case of damped structures, this has lead to the Modal Strain Energy method [7].

Damped modes can be considered as elastic models with an external damping load. Static correction for the effects of damping loads can then be incorporated. The first order correction given by

$$[T] = \left[[T_0] \quad \left[[K]_0^{-1} [K_{vi}[\phi_{1:NM}]] \right] \right] \tag{6}$$

has been shown to much more accurate prediction than a simple modal base in numerous occasion [3, 8, 4] and is used for simulations performed here. Other multi-model approaches are discussed [9] and used in some of the simulations presented here.

4 Using poles for correlation

4.1 Spectral decomposition theory

In analysis complex modes are classically defined as non trivial solutions of the homogeneous frequency response problem. That is left $\{\psi_{jL}\}$ and right $\{\psi_{jR}\}$ modeshapes associated with unique poles λ_j that verify the generalized non linear eigenvalue problem associated with a viscoelastic model

$$[Z(\lambda_j, G(\lambda_j))]\{\psi_{jR}\} = \{0\} \ \ and \ \ \{\psi_{jL}\}^T[Z(\lambda_j)] = \{0\}. \tag{7}$$

For analytic representations of the modulus, one can generally rewrite (7) as a higher order (quadratic or more), but linear, problem. The use of analytical representations of G however requires the solution of an inverse problem to *fit* the raw modulus measurement which is an error prone process. Direct uses of the complex modulus measurements is preferred by the authors but this too may be subject to bias in the dynamic material testing process [10].

Under the very unrestrictive assumption that the moduli are analytic functions, one knows that $Z(s)$ and its inverse are also analytic so that near a given isolated λ_j one has

$$[Z(s)]^{-1} = \frac{\{\psi_{jR}\}\{\psi_{jL}\}^T}{\alpha_j (s - \lambda_j)} + O(1) \tag{8}$$

where the normalization coefficient α_j depends on the choice of a norm when solving (7) and is determined by

$$\alpha_j = \{\psi_{jL}\}^T \left[\frac{\partial [Z(s)]}{\partial s}\bigg|_{\lambda_j} \right] \{\psi_{jR}\} \tag{9}$$

For symmetric $Z(s)$, the left and right complex modes are equal. For the particular case of a model of a fixed hysteretic damping ratio $Z(s) = Ms^2 + K + iB$, one normally verifies that rigid body modes are in the null space of $[B]$, and can normalize complex modes such that $\psi_j^T[M]\psi_k = \delta_{jk}$ so that the transfer is given by

$$H(s) - \sum \frac{c\phi_{jRB}\phi_{jRB}^T b}{s^2} = \sum_{j=RB+1}^{NM} \frac{\{c\psi_{jR}\}\left\{\psi_{jL}^T b\right\}}{s^2 - \lambda_j^2} = \sum_{j=RB+1}^{NM} \frac{\{c\psi_{jR}\}\left\{\psi_{jL}^T b\right\}}{2\lambda_j(s - \lambda_j)} + \frac{\{c\psi_{jR}\}\left\{\psi_{jL}^T b\right\}}{-2\lambda_j(s + \lambda_j)} \tag{10}$$

This model is not physical in the sense than poles with negative imaginary parts are unstable ($-\lambda_j$ rather than $\bar{\lambda}_j$). This implies that the static computations biased. Physically the complex modulus for negative values of ω should be the conjugate of that for positive values of ω and the loss factor should be zero at $\omega = 0$. A modal synthesis that is consistent with this hypothesis would thus use

$$H(s) = \sum \frac{R_{RB}}{s^2} + [c][K_{flex}]^{-1}[b] + \sum_{j=RB+1}^{NM} \frac{s^2 R_j}{2\lambda_j^3(s-\lambda_j)} + \frac{s^2 \bar{R}_j}{2\bar{\lambda}_j^3(s-\bar{\lambda}_j)} \tag{11}$$

with $R_j = \{c\psi_{jR}\}\left\{\psi_{jL}^T b\right\}$. The later formula is also consistent for a model with both viscous and hysteretic damping.

These spectral decompositions being unique can be used in both test and analysis to characterize damping levels associated with specific modes. In simple well controlled configurations, one can directly relate the complex modulus and the pole damping. This is in particular used for the Oberst beam testing methodology and its variants [11, 12]. For more complex structures, the correlation is not straight forward as will be illustrated next.

Figure 6 shows the location of poles when a constant complex modulus is varied in the on the edges of the design square given by $E = [4MPa - 8MPa]$ and $\eta = [.5, 1.3]$. The figure clearly indicates a non-linear relation between the modulus value and the pole.

The first two modes (7,8) cross so that proper tracking is nearly impossible. For the heavily damped modes (13,14) and the lightly damped one (9) the mapping is fairly regular so that one could reasonably relate an experimentally measured pole and the associated modulus. There are however other poles with light damping in the same range so that extracting the poles of the heavily damped modes may not be possible. For more intricate relations, poles (10,11), there is no unique value of the modulus leading to a single pole.

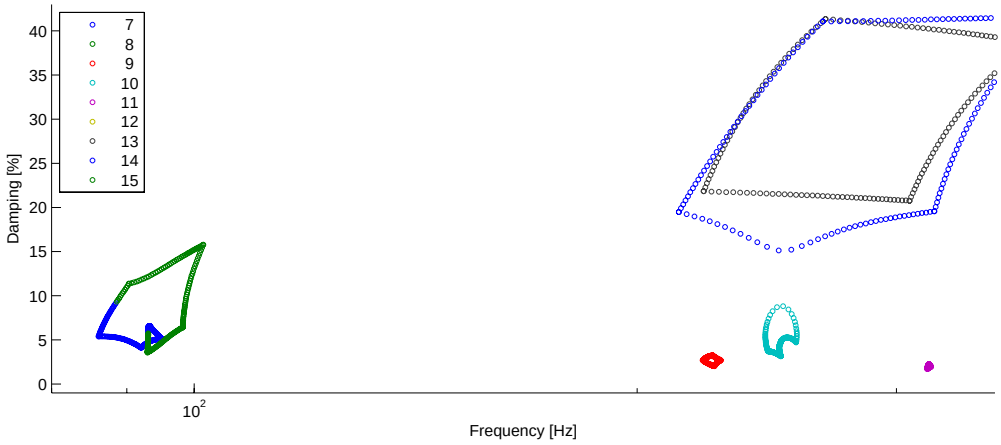

Figure 6: Pole tracking for a square variation of modulus and loss factor (slice model).

For test or when using frequency dependent moduli, the poles cannot be determined from an eigenvalue problem but must be deduced from particular transfers that are either measured or computed. Figure 7 illustrates a computation where four modes are active. One of the modes is particularly difficult to track since it heavily damped and its frequency passes the frequency of a less heavily damped mode.

4.2 Extracting poles from test or analysis transfers

While pole correlation may not be the perfect tool is remains one of the first criteria for a quantitative correlation of damping predictions. Extracting these values is thus deemed critical. This section illustrates the use of modal filters for this extraction but also shows its limits.

Modal filters [13, 14] can be used to combine measurements into responses where one particular mode is more specifically excited or observed. The idea behind this methodology is the dual for observation of what modal appropriation is to excitation with multiple shakers [15]. In the present case modes are not known, but one can use the normal modes of a reference elastic structure (with some reference modulus of each of the viscoelastic materials) to build the modal filters. Figure 7 clearly shows in this simulation that the peaks are perfectly separated by this approach.

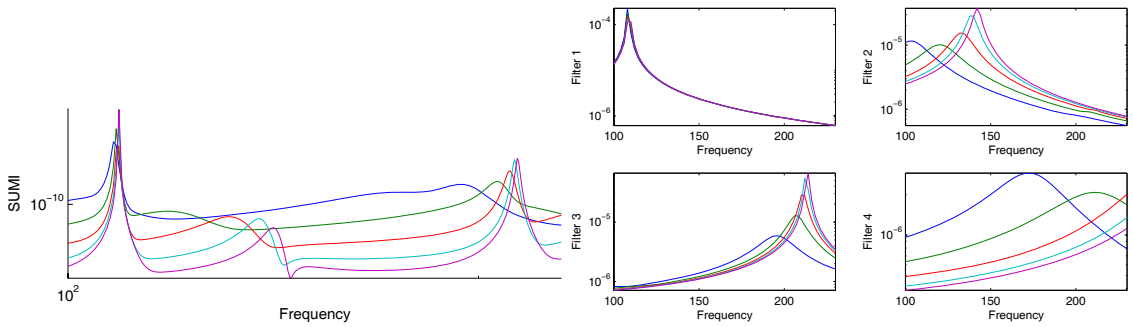

Figure 7: Sum of the imaginary part of transfers (left) and modal filters (right) (frame model).

When applied to test data, the modal filter results are quite good for the first modes as shown in figure 8. In higher frequencies results become poor. The reason for this is illustrated by the test auto-MACS shown in figure 9. This figure clearly indicate that only the first modes are well separated in shape (later there a significant off-diagonal terms for modes that are close in frequency). These are limitations of the test configuration but illustrate the fact that, in this application, one was interested in predicting and validating predictions in a much broader range than what is usually considered for modal analysis.

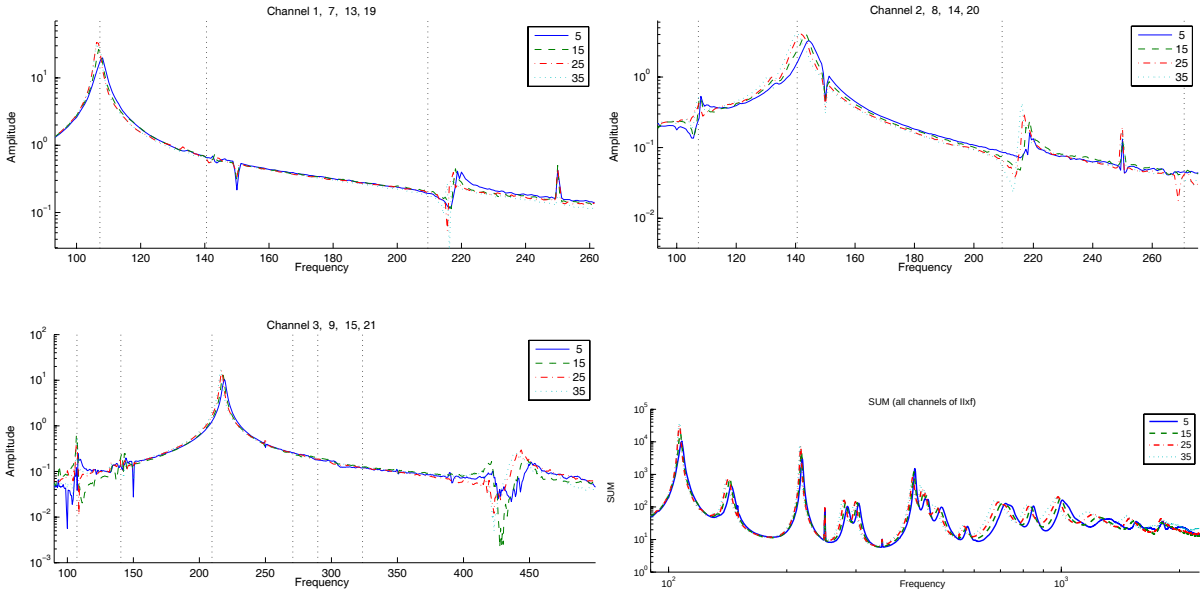

Figure 8: Frame test. Top : Modal filter for mode 2. Bottom : sum of responses.

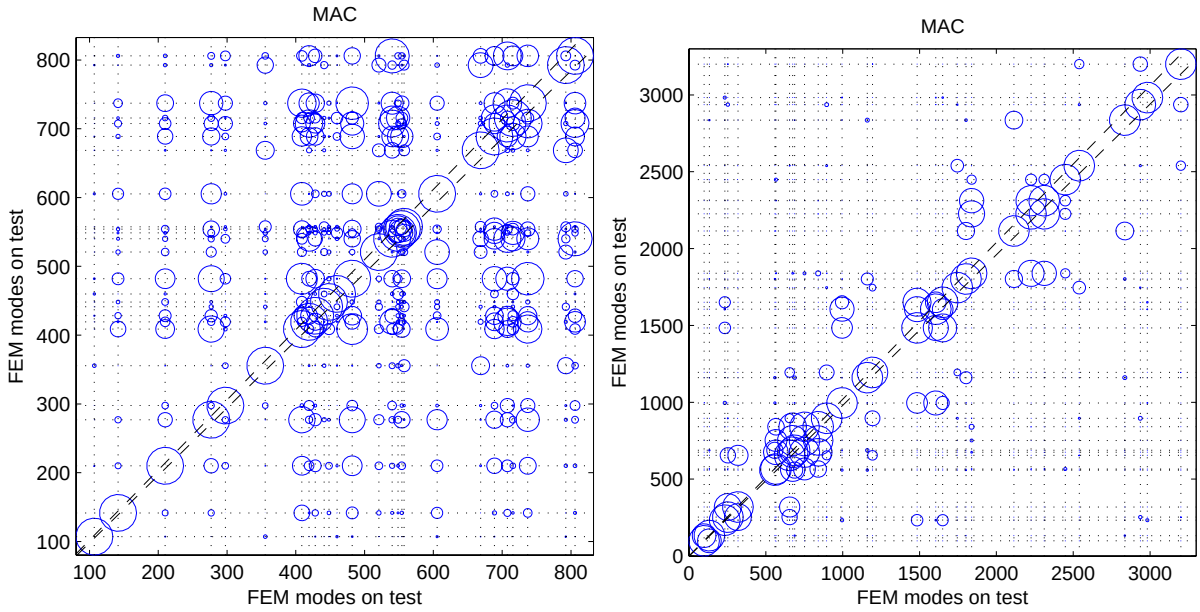

Figure 9: Auto MAC of FEM modes on sensors with indication of frequency. Left : frame. Right : slice.

For analysis, modal filters can be used to estimate damping levels more efficiently since one can use both input and output filtering. Figure 10 illustrates the gradual rise of damping with frequency in the considered application which is the basis of the proposed design.

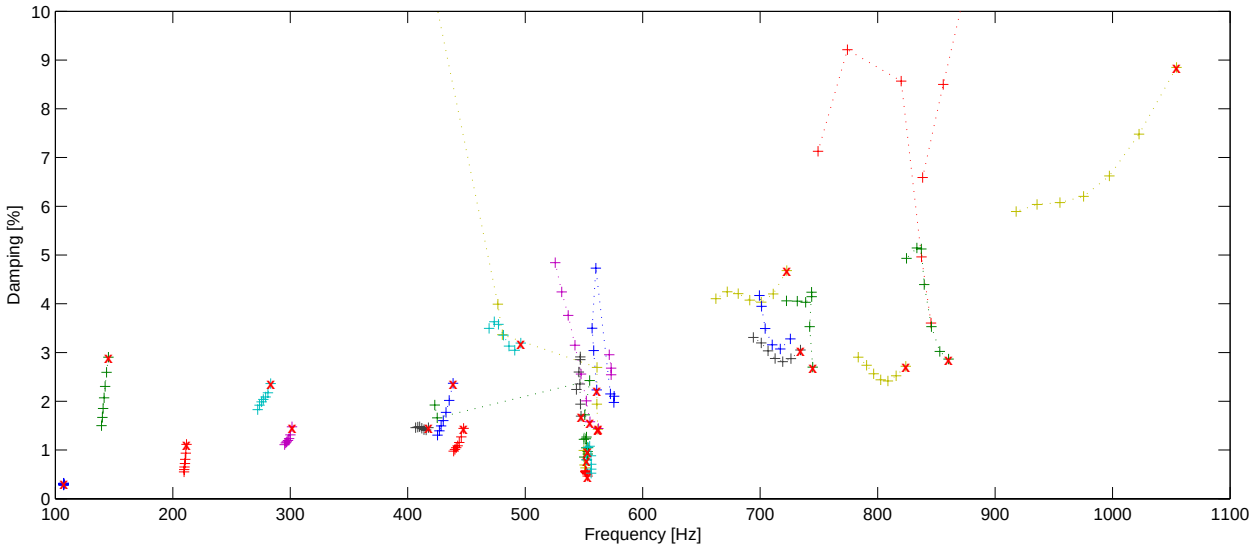

Figure 10: Pole tracking for the frame model.

4.3 Identification limits for highly damped and close modes

The preceding section showed that heavy damping and close frequencies posed a significant challenge. This was also found to induce difficulties in identification procedures. This section points fundamental reasons for this fact.

In practical cases, parameters estimation is performed using data from a restricted frequency band. Given an estimated model order, one solves the non-linear output-error minimization problem [16]

$$([R_n], \lambda_n) = \underset{[R_n],\Lambda_n}{\text{ArgMin}} \left(\sum_{\omega_{min}}^{\omega_{max}} \left\| H_t(\omega_s) - \sum_{\text{Im}(\lambda_n)>\omega_{min}}^{\text{Im}(\lambda_n)<\omega_{max}} \frac{R_n}{j\omega_s - \lambda_n} + \frac{\bar{R}_n}{j\omega_s - \bar{\lambda}_n} - F + \frac{G}{\omega_s^2} \right\|^2 \right), \qquad (12)$$

where F and G are the high and low frequency residuals and the mode residues have the form discussed in section 4.

When damping is high and poles relatively close, the conditioning of this problem deteriorates rapidly which induces a lack of precision on damping estimates. To illustrate this point, one uses the simple 8 DOF test shown in figure 11. All masses are set to 1 Kg, exept for DOF 7 and 8, were masses are set to 10 Kg. Stiffness, shown on the figure 11, are respectively k_1=1e4 N.m^{-1}, k_2=1e5 N.m^{-1}, and k_3=5e7 N.m^{-1}. Viscous damping d will vary from 1 to 25 N.m^{-1}.s. Frequencies ω_n and damping ratios ζ_n for the extreme values of d are given in the table of figure 11. Free-free sine mode-shapes have been applied to computed complex mode to simulate measurements. Hence, the simulated frequency response function H between an input b and an output c_k is given by

$$H_k(s) = \sum_{n=1}^{8} \left(\frac{\{c_k\}[\psi_n][\psi_n]^T\{b\}}{(s-\lambda_n)} + \frac{\{c_k\}[\bar{\psi}_n][\bar{\psi}_n]^T\{b\}}{(s-\bar{\lambda}_n)} \right). \qquad (13)$$

with $\{c_k\} = \{sin(\pi k)\ ...\ sin(n\pi k)\}$, $k \in [0,1]$, $\{b\} = \{0\ 1\ 0\ ...0\}^T$ and $\lambda_n = \omega_n \left(j - \sqrt{1-\zeta^2} \right)$.

For each viscous damping coefficient d, a state space model is assembled. Frequencies, damping ratios and complex modes and FRF are computed and used as *measurements* in this illustration.

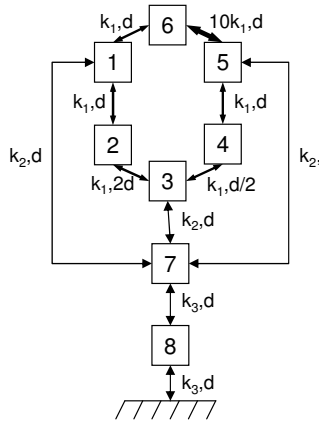

A. Connectivity between the 8 DOF of the model

d=1 N.m^{-1}.s

Frequency (Hz)	Damping (%)
90.6901	0.48685
97.4868	0.6817
152.2651	0.27863
234.6602	0.46333
245.9542	0.4266
329.7354	0.10011
375.0836	0.2902
811.8541	0.014084

d=25 N.m^{-1}.s

Frequency (Hz)	Damping (%)
91.9862	8.2824
95.5752	15.139
151.8816	5.5511
232.7833	9.3533
244.6676	8.4768
329.4132	1.8795
373.5898	5.8432
811.8329	0.28087

B - Frequencies and damping ratios for extrema values of viscous damping d

Figure 11: Numerical test case

For identification, one considers the 200-280Hz band which contains the fourth and fith modes (see table11.B). For given values of poles 4 and 5 exact damping ($d = 17$) is used and the frequency is varied in a [-8% ; 8%] range. Since the poles are given, the minimization of (12) is a linear least squares problem that gives the residues.

Figure 12 shows a map of the objective function for the range of frequency values. One first notes the presence of two local minima meaning that the output error minimization problem (12) has non-unique solutions. Further studies have shown that this split is observed for high damping compared to separation. This condition can be evaluated using the modal overlap criterion [17] : for 2 modes j and k, when $2\zeta_j\omega_j \approx |\omega_j - \omega_k|$ then damping can be considered high compared to frequency separation.

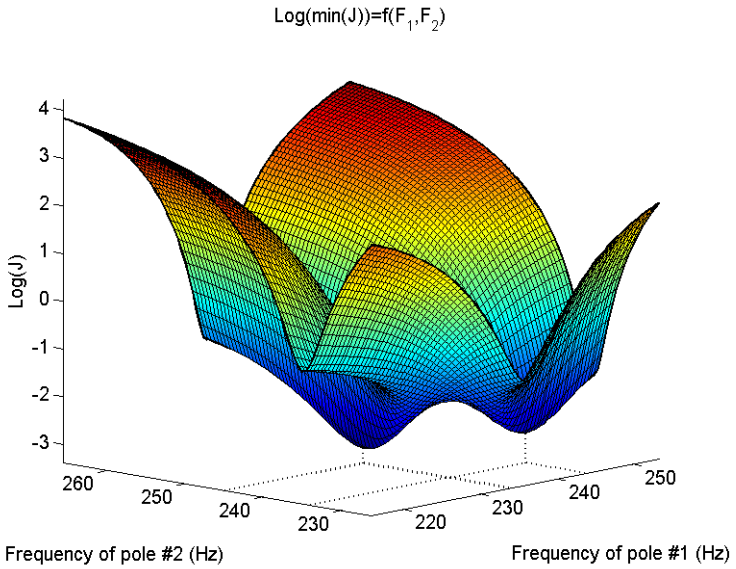

Figure 12: Log(Min(J)) for F_4 and F_5 within [-8% ; 8%]

Figure 13 overlays the analytical pole value, the frequency at which the minimum of the cost function is observed when the pole frequency is varied for the exact damping ratio, the uncertainty range defined as the range of frequencies for which the cost is less than 2% higher than the minimum.

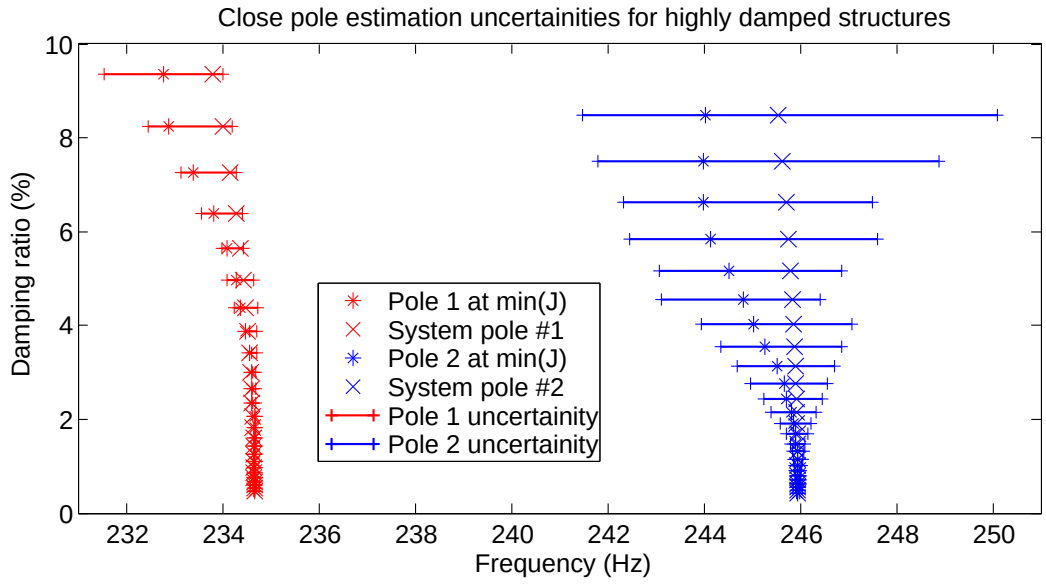

Figure 13: True pole VS found poles. Pole locations for the cost function J within [Min(J) Min(J)*1.02] is also presented

These illustrations clearly indicate that when damping increases the level of bias and uncertainty in the output error solution augments drastically. Modal extraction is thus fundamentally difficult in such situations.

5 Conclusion

This study has shown that modeling techniques for structures containing viscoelastic materials are well mastered and lead to reasonable test/analysis correlation. Material characterizations that properly include frequency and temperature dependence remain a key difficulty and in most situations one cannot expect to find a simple relation between a pole and the modulus value at the associated frequency. Pole extraction is further made more difficult by the presence of damping. Modal filter techniques have been found to help but fail when the modal density increases. Finally identification techniques have been shown to have unicity and bias problems in the same situation. Many questions are thus left unanswered and will be the object of further study.

References

[1] Balmes, E., *Viscoelastic vibration toolbox, User Manual*, SDTools, 2004.

[2] Balmes, E. and Germès, S., "Design strategies for viscoelastic damping treatment applied to automotive components," *IMAC, Dearborn*, 2004.

[3] Plouin, A. and Balmes, E., "A test validated model of plates with constrained viscoelastic materials," *International Modal Analysis Conference*, 1999, pp. 194–200.

[4] Balmes, E., "Modes and Regular Shapes. How to Extend Component Mode Synthesis Theory." *Proceedings of the XI DINAME - Ouro Preto - MG - Brazil*, March 2005.

[5] Rubin, S., "Improved Component-Mode Representation for Structural Dynamic Analysis," *AIAA Journal*, Vol. 13, No. 8, 1975, pp. 995–1006.

[6] MacNeal, R., "A hybrid method of component mode synthesis," *Computers and structures*, Vol. 1, No. 4, 1971, pp. 581–601.

[7] Rogers, L., Johson, C., and Keinholz, D., "The Modal Strain Energy Finite Element Method and its Application to Damped Laminated Beams," *Shock and Vibration Bulletin*, Vol. 51, 1981.

[8] Bobillot, A., *Méthodes de réduction pour le recalage. Application au cas d'Ariane 5*, Ph.D. thesis, École Centrale Paris, 2002.

[9] Balmes, E., "Parametric families of reduced finite element models. Theory and applications," *Mechanical Systems and Signal Processing*, Vol. 10, No. 4, 1996, pp. 381–394.

[10] van't Hof, C., Mohanty, P., and Rixen, D., "Testing a Dynamic Mechanical Analyzer: influence of the measuring column dynamics," *IMAC*, 2003.

[11] Oberst, H. and Frankenfeld, K., "Über die Dämpfung der Biegeschwingungen dünner Bleche durch festhaftende Beläge," *Acustica*, Vol. 2, 1952, pp. 181–194.

[12] Nashif, A., Jones, D., and Henderson, J., *Vibration Damping*, John Wiley and Sons, 1985.

[13] Shelley, S., Allemang, R., Slater, G., and Shultze, J., "Active Vibration Control Utilizing an Adaptive Modal Filter Based Modal Control Method," *International Modal Analysis Conference*, 1993, pp. 751–758.

[14] Deraemaeker, A. and Preumont, A., "Modal filters for vibration based damage detection," *ISMA*, 2004, pp. 501–513.

[15] Balmes, E., Chapelier, C., Lubrina, P., and Fargette, P., “An evaluation of modal testing results based on the force appropriation method,” *International Modal Analysis Conference*, 1995, pp. 47–53.

[16] Balmes, E., “Frequency domain identification of structural dynamics using the pole/residue parametrization,” *International Modal Analysis Conference*, 1996, pp. 540–546.

[17] Hasselman, T., “Modal Coupling in Lightly Damped Structures,” *AIAA Journal*, Vol. 14, No. 11, 1976, pp. 1627–1628.